Unimolecular Dissociation of the CH_3OCO Radical: An Intermediate in the $CH_3O + CO$ Reaction†

Laura R. McCunn, Kai-Chung Lau, Maria J. Krisch, and Laurie J. Butler*

The James Franck Institute and Department of Chemistry, The University of Chicago, Chicago, Illinois 60637

Jieh-Wen Tsung and Jim J. Lin

Institute of Atomic and Molecular Sciences, Academia Sinica, Taipei 106, Taiwan

Received: July 31, 2005; In Final Form: September 29, 2005

This work investigates the unimolecular dissociation of the methoxycarbonyl, CH_3OCO, radical. Photolysis of methyl chloroformate at 193 nm produces nascent CH_3OCO radicals with a distribution of internal energies, determined by the velocities of the momentum-matched Cl atoms, that spans the theoretically predicted barriers to the $CH_3O + CO$ and $CH_3 + CO_2$ product channels. Both electronic ground- and excited-state radicals undergo competitive dissociation to both product channels. The experimental product branching to $CH_3 + CO_2$ from the ground-state radical, about 70%, is orders of magnitude larger than Rice−Ramsperger−Kassel−Marcus (RRKM)-predicted branching, suggesting that previously calculated barriers to the $CH_3OCO \rightarrow CH_3 + CO_2$ reaction are dramatically in error. Our electronic structure calculations reveal that the cis conformer of the transition state leading to the $CH_3 + CO_2$ product channel has a much lower barrier than the trans transition state. RRKM calculations using this cis transition state give product branching in agreement with the experimental branching. The data also suggest that our experiments produce a low-lying excited state of the CH_3OCO radical and give an upper limit to its adiabatic excitation energy of 55 kcal/mol.

Introduction

This paper investigates the dissociation dynamics of the methoxycarbonyl radical, CH_3OCO, produced by the 193 nm photolysis of methyl chloroformate. This radical serves as the intermediate along the reaction coordinate for the reaction of the methoxy radical with carbon monoxide, $CH_3O + CO \rightarrow CH_3 + CO_2$. This reaction is important because of its relevance to the fate of methoxy radicals in atmospheric reactions and hydrocarbon combustion.[1,2] Furthermore, the potential energy surface for this reaction is similar to that of the reaction $HO + CO \rightarrow H + CO_2$, which proceeds via the analogous HOCO intermediate. While the $HO + CO$ system has been the subject of numerous investigations,[3−7] there are comparatively few studies on the $CH_3O + CO$ system.

The kinetics of the $CH_3O + CO$ reaction has been investigated previously. In the course of experiments on $CH_3O + NO$, Wiebe and Heicklen performed photolysis of methyl nitrate in the presence of N_2 and CO to verify if the reaction would produce CO_2.[8] Indeed, they did observe CO_2 formation, but could not accurately measure a rate constant, saying only that the removal rate of CH_3O by CO is approximately 5×10^{-4} slower than removal by NO in the temperature range 25−150 °C. They theorized that the principal products of $CH_3O + CO$ could be $(CH_3O)_2CO$ or $(CH_3OCO)_2$. Sanders et al. also principally studied the $CH_3O + NO$ reaction but looked at the reaction of CH_3O with CO and found it too slow to measure the rate constant.[9] They suggested an upper bound of $\log k = 6.7\ M^{-1}\ s^{-1}$ for the reaction of $CH_3O + CO$. Lissi et al. used thermal decomposition of dimethyl peroxide in the presence of CO at 123−153 °C to measure the $CH_3O + CO \rightarrow CH_3 + CO_2$ rate constant.[10] Their results showed that $E_a = 11.8 \pm 1.5$ kcal/mol for the reaction. Wantuck et al. measured removal of CH_3O by CO at 473−973 K and found that the rate could not be described by a simple Arrhenius expression.[11] They expected $CH_3 + CO_2$ to be the major products but suggested that a minor $HCO + H_2CO$ product channel may arise at high temperatures. Tsang and Hampson compiled the results of the above experiments in a kinetic database for combustion chemistry and recommended the value of $E_a = 11.8 \pm 1.5$ kcal/mol found by Lissi et al. with an uncertainty factor of at least 5.[12]

More recently, several theoretical studies have been published concerning the $CH_3O + CO$ system. Francisco studied the $CH_3O + CO$ reaction, considering only the $CH_3 + CO_2$ product channel via the CH_3OCO intermediate.[13] His QCISD(T)/6-311++G(3df,3pd) calculations predicted an entrance channel barrier of 5.8 kcal/mol and a barrier of 38.2 kcal/mol for the $CH_3OCO \rightarrow CH_3 + CO_2$ channel. Kang and Musgrave also calculated the $CH_3OCO \rightarrow CH_3 + CO_2$ reaction barrier while testing their newly developed KMLYP hybrid density-functional method.[14] Their value of 39.5 kcal/mol agreed with Francisco's result.

Zhou et al. investigated the multichannel $CH_3O + CO$ reaction at the B3LYP/6-311++G** level of theory.[15] For dissociation of the CH_3OCO radical, they found the $CH_3O + CO$ channel to have a 19.5 kcal/mol barrier and the $CH_3 + CO_2$ channel to have a 27.0 kcal/mol barrier. The other product channels examined were $H_2CO + HCO$ and $H_2CCO + OH$, but both had higher barriers (38.9 and 35.0 kcal/mol, respectively) than the $CH_3 + CO_2$ channel. A direct abstraction

† Part of the special issue "William Hase Festschrift".

* L-Butler@uchicago.edu.

10.1021/jp054238r CCC: $33.50
Published on Web 00/00/0000 PAGE EST: 10

reaction of $CH_3O + CO \rightarrow H_2CO + HCO$ was also found, with a barrier of 17.16 kcal/mol relative to the reactants.

Wang et al. used the G2(B3LYP/MP2/CC) method to study the $CH_3O + CO$ reaction and also completed multichannel Rice−Ramsperger−Kassel−Marcus (RRKM) calculations for a wide range of temperatures and pressures.[16] They predicted a 6.39 kcal/mol barrier for the $CH_3O + CO$ addition reaction leading to the CH_3OCO intermediate and a 32.3 kcal/mol barrier, measured from the zero point level of the radical intermediate, for the radical's dissociation to $CH_3 + CO_2$. Examination of the transition state for this dissociation led them to assert that Francisco had misidentified the $CH_3OCO \rightarrow CH_3 + CO_2$ transition state, making his barrier energy too high. Interestingly, they suggested strong CH_3 tunneling in the decomposition of $CH_3OCO \rightarrow CH_3 + CO_2$, due to the transition state's abnormally large imaginary frequency. In their calculations, they included the radical dissociation pathways to $H_2CO + HCO$ and $H_2CCO + OH$ as well as the direct reaction of $CH_3O + CO \rightarrow H_2CO + HCO$. The RRKM results showed that under atmospheric conditions, the stabilization of the CH_3OCO radical would dominate. Under combustion conditions, the major products would be $H_2CO + HCO$, from the direct abstraction channel. The same group later studied the mechanism of the $H_2CCO + OH$ reaction.[17] They predicted $CO + CH_2OH$ to be the major products at lower temperatures, while $H_2O + HCCO$ would dominate at higher temperatures. Referencing their previous work on $CH_3O + CO$, they showed that the CH_3OCO radical intermediate would play a very minor role in the $H_2CCO + OH$ reaction.

The CH_3OCO radical could also serve as one of many possible intermediates in the vinyl $+ O_2$ reaction. G2M(RCC, MP2) and multichannel RRKM calculations by Mebel et al. showed that the most favorable reaction pathway for this system leads to $CHO + H_2CO$.[18] As part of a minor channel, the CH_3OCO radical can dissociate to make $CH_3 + CO_2$, but the $CH_3O + CO$ products were not included in the analysis. The barrier for $CH_3OCO \rightarrow CH_3 + CO_2$ at the B3LYP/6-311G(d,p) level of theory was found to be 27.1 kcal/mol, a result similar to that of Zhou et al.[15]

Figure 1 shows the energetics for the $CH_3O + CO \rightarrow CH_3 + CO_2$ reaction at various levels of theory as calculated by Francisco,[13] Wang et al.[16] and Zhou et al.[15] The calculated overall reaction enthalpies are in agreement, as well as the predicted barrier heights for $CH_3OCO \rightarrow CH_3O + CO$. In contrast, the energies for the $CH_3OCO \rightarrow CH_3 + CO_2$ transition state differ by up to 10 kcal/mol. The large discrepancy in the values calculated for the barrier to the $CH_3O + CO_2$ channel warrants more experimental efforts on the CH_3OCO radical. The original motivation for the experiments presented here was thus to measure a branching ratio between the two dissociation channels of the methoxycarbonyl radical and compare it to the RRKM-predicted branching ratios based on these published barrier heights.

The experiments described in this paper utilize methyl chloroformate, $CH_3OC(O)Cl$, as a photolytic precursor for the radical. This precursor and the photolysis wavelength of 193 nm were deliberately chosen to produce nascent CH_3OCO radicals with an internal energy range that spans the theoretically predicted dissociation barriers shown in Figure 1. Listed below are the reactions that are energetically possible for methyl chloroformate at 193 nm, with the dissociation pathways open to CH_3OCO radicals and other photolytic fragments indented (reactions 1−12). Reliable values for the enthalpies of reactions 6, 8, and 11 could not be found in the literature, so we calculated them by the G3//B3LYP method with Gaussian 98.[19] For reaction 1, we used both G3//B3LYP and CCSD(T) as described in the Experimental Method section to calculate the C−Cl bond energy for both cis and trans conformers of methyl chloroformate. All the results are summarized in Table 1, while only the G3//B3LYP value for the most stable CH_3OCOCl and CH_3OCO conformers is shown in the list below.

TABLE 1: Theoretical $D_0(CH_3OC(O)\cdots Cl)$ at the G3//B3LYP and CCSD(T) Levels of Theory in kcal/mol[a]

	G3//B3LYP	CCSD(T)[b]
D_0(*cis*-$CH_3OC(O)-Cl$)	85.4	84.6
D_0(*trans*-$CH_3OC(O)-Cl$)	81.3	80.3

[a] The D_0 calculations correspond to reactions where *cis*- or *trans*-$CH_3OC(O)Cl$ is dissociated into *cis*-$CH_3OCO + Cl$. The G3//B3LYP results in this table also refer to the *cis*-CH_3OCO radical intermediate for consistency, though the trans conformer is predicted to have the minimum energy at that level of theory. Note that *cis*-$CH_3OC(O)Cl$ is approximately 4 kcal/mol lower in energy than the trans conformer. [b] Based on the CCSD(T)/6-311G(2df,p) optimized geometries, single-point energies were calculated at the CCSD(T)/aug-cc-pV(Q+d)Z level of theory. Zero-point vibrational energy correction and core-valence electronic correlations were included (see Experimental Method section).

$$CH_3OC(O)Cl \rightarrow CH_3OCO + Cl \qquad \Delta H_{0\ K} = 85.2\ \text{kcal/mol} \quad (1)$$

$$CH_3OCO \rightarrow CH_3O + CO \qquad \Delta H_{0\ K} = 15.0\ \text{kcal/mol}^{16} \quad (2)$$

$$CH_3OCO \rightarrow CH_3 + CO_2 \qquad \Delta H_{0\ K} = -22.54\ \text{kcal/mol}^{16} \quad (3)$$

$$CH_3OCO \rightarrow H_2CO + HCO \qquad \Delta H_{0\ K} = 19.75\ \text{kcal/mol}^{16} \quad (4)$$

$$CH_3OCO \rightarrow H_2CCO + OH \qquad \Delta H_{0\ K} = 35.84\ \text{kcal/mol}^{16} \quad (5)$$

$$CH_3OC(O)Cl \rightarrow CH_3 + OC(O)Cl \qquad \Delta H_{0\ K} = 86.3\ \text{kcal/mol} \quad (6)$$

$$OC(O)Cl \rightarrow CO_2 + Cl \qquad \Delta H_{0\ K} = -37.4\ \text{kcal/mol}^{20} \quad (7)$$

$$CH_3OC(O)Cl \rightarrow H_2CO + HC(O)Cl \qquad \Delta H_{0\ K} = 24.4\ \text{kcal/mol} \quad (8)$$

$$HC(O)Cl \rightarrow HCl + CO \qquad \Delta H_{0\ K} = -10.8\ \text{kcal/mol}^{21} \quad (9)$$

$$H_2CO \rightarrow H_2 + CO \qquad \Delta H_{0\ K} = 1.3\ \text{kcal/mol}^{22} \quad (10)$$

$$CH_3OC(O)Cl \rightarrow H_2CO + HOCCl \qquad \Delta H_{0\ K} = 71.2\ \text{kcal/mol} \quad (11)$$

$$HOCCl \rightarrow HCl + CO \qquad \Delta H_{0\ K} = -58.9\ \text{kcal/mol}^{23} \quad (12)$$

In these experiments, photolysis of methyl chloroformate produces Cl atoms and momentum-matched CH_3OCO radicals that are dispersed by their recoil translational energy and thus by the radicals' internal energy. Measurement of the recoil velocities of Cl atoms alone determines the total recoil translational energy distribution, and by energy conservation, the internal energy distribution of the momentum-matched

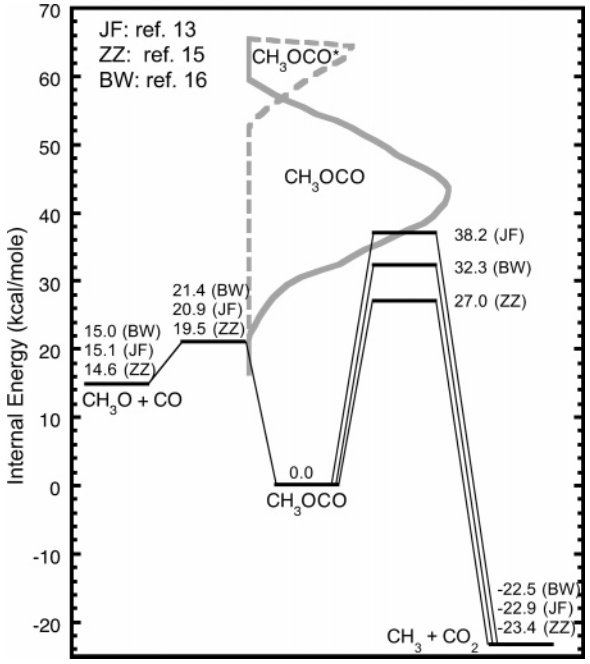

Figure 1. Energetics of the $CH_3O + CO \rightarrow CH_3 + CO_2$ reaction. The numbers are computational results from refs 13, 15, and 16. JF stands for QCISD(T)/6-311++G(3df,3pd) values (ref 13). ZZ stands for B3LYP/6-311++G** values (ref 15). BW stands for G2(B3LYP/MP2/CC) values (ref 16). Overlaid is the internal energy distribution of the nascent CH_3OCO radicals produced in the 193 nm photolysis of methyl chloroformate, as determined from the fitting of the data in Figure 3. The solid line is the distribution belonging to ground-state radicals, while the dashed line represents radicals assigned to an excited state.

CH_3OCO radicals. These experiments also measure the velocity distributions of the products from dissociation of energetic CH_3OCO radicals, allowing us to probe the dissociation dynamics of the radicals and to measure a product branching ratio.

Experimental Method

A. Molecular Beam Scattering Experiments. The velocities of the primary photofragments and the products of the unimolecular dissociation of the CH_3OCO radicals were measured with the rotating-source crossed laser-molecular beam apparatus on the 21A1 U9/Chemical Dynamics Beamline at the National Synchrotron Radiation Research Center in Hsinchu, Taiwan. Details of the experimental apparatus have been described previously.[24] A 10% methyl chloroformate-He molecular beam was created by bubbling He (800 Torr total backing pressure) through methyl chloroformate (97% purity, Aldrich) cooled to 16 °C and expanding it through an Even-Lavie (type E.L.-5-3-2000) pulsed valve with a 0.25 mm orifice operating at 40 Hz. The nozzle was heated to 107 °C to reduce cluster formation. The molecular beam of the parent molecule was characterized by directing the beam through a chopper wheel along the detector axis. The measured number-density speed distribution of the methyl chloroformate molecular beam for the data presented here was typically peaked at 1.18×10^5 cm*sec^{-1} with a full width at half-maximum of 27%.

Photodissociation was accomplished with a Lambda Physik LPX 210i excimer laser operating at the 193.3 nm ArF transition. The laser ran at 40 Hz with a pulse energy between 80 and 150 mJ/pulse. The pulse energy varied over the course of our experiments, but a specific value was recorded for each individual spectrum. The laser beam was focused to an area of 2.1 mm wide by 8.9 mm high, intersecting the ~3 mm high molecular beam at a 90° angle in the interaction region. Photofragments recoiling in the direction of the detector traveled 10.05 cm to the ionizing region, where tunable VUV synchrotron radiation ionized a portion of the fragments. Photoionization energies were selected by tuning the gap of a U9 undulator, which generated the radiation. For example, Cl^+ data were collected at $m/e = 35$ using a 14.8 eV photoionization energy, requiring a 34 mm undulator gap. Unwanted higher harmonics of VUV radiation were removed by a rare gas filter. The VUV beam was defined by a circular aperture of 7 mm diameter for a full-width at half-maximum of 0.27 eV, or 3%.

Ionized photofragments were mass-selected by an Extrel 1.7 MHz quadrupole mass spectrometer and then counted by a Daly detector. A multichannel scaler was used to record the total time of flight (TOF) of the photofragments from the interaction region to the detector. Recoil translational energy distributions were found by forward convolution fitting of the TOF spectra. The forward convolution fitting of the data takes into account the ion flight time, derived from the apparatus' ion flight constant of 5.45 μs·amu$^{-1/2}$. The experimental data and fits shown in this paper have already subtracted the 1.6 μs delay between the trigger of the multichannel scaler and the arrival of the laser pulse at the interaction region.

The absorption spectrum of methyl chloroformate presented in this paper was collected on a Hewlett-Packard 8453 UV/visible spectrophotometer. The spectrum was taken on the vapor in the headspace above a liquid sample. The sample cuvette and spectrophotometer were flushed with nitrogen to prevent absorption of UV light by oxygen in the air.

B. Theoretical Calculations. The $D_0(CH_3OC(O)\cdots Cl)$, the transition barrier heights involved in dissociation reactions ($CH_3OCO \rightarrow CH_3O + CO$ and $CH_3OCO \rightarrow CH_3 + CO_2$), and the isomerization barrier between *cis*-CH_3OCO and *trans*-CH_3OCO were calculated by the G3//B3LYP method.[25] We also evaluated the D_0 and transition/isomerization barrier heights at the coupled cluster level with single and double excitations plus a quasi-perturbative triple excitation [CCSD(T)][26−28] together with Dunning's correlation consistent basis sets.[29,30] Specifically, the geometries of *cis*-/*trans*-$CH_3OC(O)Cl$, *cis*-/*trans*-CH_3OCO, CH_3O, CH_3, CO_2, CO and the transition states were optimized at the CCSD(T)/6-311G(2df,p) level. Based on the optimized structures, single-point frozen core energy calculations were carried out at the CCSD(T)/aug-cc-pV(Q+d)Z level of theory. The calculations include a zero-point vibrational energy (ZPVE) correction at the minimum and transition state structures using the harmonic vibrational frequencies at the CCSD(T)/6-311G-(2df,p) level. The core-valence electron correlation (1s electrons on C and O, 2s/2p electrons on Cl) was obtained at the CCSD-(T) level using the cc-pwCVTZ basis set.[31] The G3//B3LYP calculations were performed with the Gaussian 03 package of programs,[32] with the exception of the enthalpies for reactions 6, 8, and 11, which were calculated separately in Gaussian 98. The CCSD(T) single-point energies and vibrational frequencies calculations were done with the program MOLPRO 2002.6.[33] Transition state identities were confirmed by intrinsic reaction coordinate calculations.

Results and Analysis

The data showed that C−Cl bond fission is the major photodissociation channel of methyl chloroformate at 193 nm. Methyl chloroformate absorbs strongly at 193 nm, as shown in the absorption spectrum in Figure 2.

C−Cl fission was evidenced by a Cl^+ time-of-flight (TOF) spectrum at $m/e = 35$ shown in Figure 3. The total recoil kinetic energy distribution $P(E_T)$ for C−Cl fission was determined by forward convolution fitting of the data. The total $P(E_T)$ is

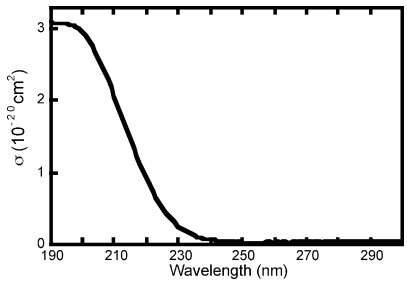

Figure 2. Gas-phase absorption spectrum of methyl chloroformate. The absorption cross section is a lower bound, as we observed the magnitude of absorbance decreasing with time. This may be due to the molecules reacting with water vapor or the walls of the cuvette.

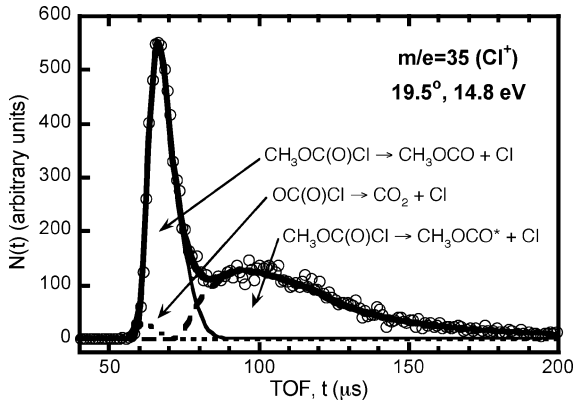

Figure 3. Time-of-flight (TOF) spectrum of $m/e = 35$ (Cl^+) taken at a source angle of 19.5° and ionization energy of 14.8 eV for 15000 laser shots. The open circles represent experimental data points, while the bold solid line is the overall forward convolution fit to the data with the $P(E_T)$ shown in Figure 4. The thin solid line corresponds to chlorine atoms that are momentum-matched to CH_3OCO radicals formed in the ground state. The dashed line corresponds to chlorine atoms that are momentum-matched to CH_3OCO radicals assigned as being formed in an excited state. The dotted line shows a contribution near 60 μs from dissociation of OCOCl radicals, as reasoned in the fitting of the CH_3 and CO_2 data shown in Figures 11 and 15.

bimodal, with the low-energy component peaking at 1 kcal/mol. Our results suggest that the low kinetic energy C−Cl bond fission channel produces CH_3OCO radicals in an excited electronic state. These data are marked by the dashed line in Figure 3 and have a $P(E_T)$ shown by the dashed line in Figure 4. The dominant, high kinetic energy, C−Cl bond fission channel produces CH_3OCO radicals in the ground electronic state as shown by the solid lines in Figures 3 and 4. The dotted line fit in Figure 3 near 60 μs arrival time shows a contribution of Cl from dissociation of OCOCl radicals (reaction 7), as explained later in this section.

The internal energy range of the nascent CH_3OCO radicals, although they all dissociate, is easily deduced from the momentum-matched Cl atom velocities using conservation of energy:

$$E_{\text{parent}} + h\nu = D_0(\text{C}-\text{Cl}) + E_{\text{int}} + E_{\text{Cl}} + E_{\text{T}}$$

This calculation was done for the entire distribution of E_T produced in our experiment, shown in Figure 4. The energy of a 193.3 nm photon, $h\nu$, is equal to 147.8 kcal/mol, including the air-to-vacuum correction. D_0(C−Cl) was calculated by G3//B3LYP and CCSD(T) methods, with the results shown in Table 1. We used the G3//B3LYP value for C−Cl bond fission leading to the most stable (trans) conformer of the radical, $D_0 = 85.2$ kcal/mol. E_{parent} is the internal energy of the methyl chloroformate molecule; we estimated it by assuming that vibrational modes are not cooled by the nozzle expansion and have equilibrated to the nozzle temperature. Using vibrational modes calculated at the B3LYP/6-31G(d) level of theory,[34] we determined the average vibrational energy of the methyl chloroformate molecule to be 2.8 kcal/mol at the 107 °C nozzle temperature used in our experiments. E_{Cl} refers to the energy of the spin−orbit state of the chlorine atoms. E_{Cl} is 0 kcal/mol if Cl is produced in the $^2P_{3/2}$ state and 2.5 kcal/mol in the $^2P_{1/2}$ state.[35] Our experiments cannot distinguish between the two spin−orbit states, but 235 nm photolysis of methyl chloroformate with resonance-enhanced multiphoton ionization detection in separate experiments revealed that both Cl($^2P_{3/2}$) and Cl($^2P_{1/2}$) are produced. The internal energy distribution of the radicals produced in our experiment is shown overlaid with the energetics of the CH_3OCO reaction in Figure 1.

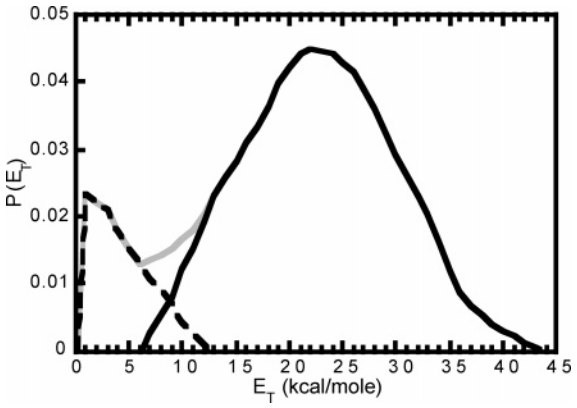

Figure 4. Recoil kinetic energy distribution, $P(E_T)$, in C−Cl bond fission derived from forward convolution fitting of the data in Figure 3. The solid gray line shows the total $P(E_T)$. The total $P(E_T)$ is divided into two subdistributions used in fitting of subsequent spectra. The black solid line corresponds to high E_T, low E_{int} CH_3OCO radicals that are formed in the ground state. The dashed line corresponds to low E_T, high E_{int} CH_3OCO radicals presumed to be in an excited state. Note that the relative contributions where they overlap are estimates only.

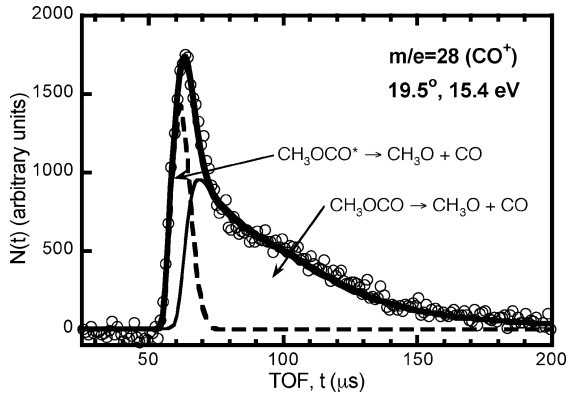

Figure 5. TOF spectrum of $m/e = 28$ (CO^+), 19.5° source angle, obtained from 100000 laser shots at an ionization energy of 15.4 eV. Open circles are experimental data, while the bold solid line is the overall fit to the data. The thin solid line shows CO produced by unimolecular dissociation of ground-state CH_3OCO radicals. This signal is fit as described in the text by the $P(E_T)$ distributions shown by the black solid lines in Figures 4 and 6. The dashed line shows CO produced by excited-state CH_3OCO radicals, fit by the dashed line $P(E_T)$s in Figures 4 and 7.

Unimolecular dissociation of the nascent CH_3OCO radicals via reaction 2 was observed in the $m/e = 28$ (CO^+) TOF shown in Figure 5. The fit accounts for the velocity imparted to the CH_3OCO radical in the initial C−Cl bond fission (reaction 1) as well as the velocity imparted during the recoil of CO from

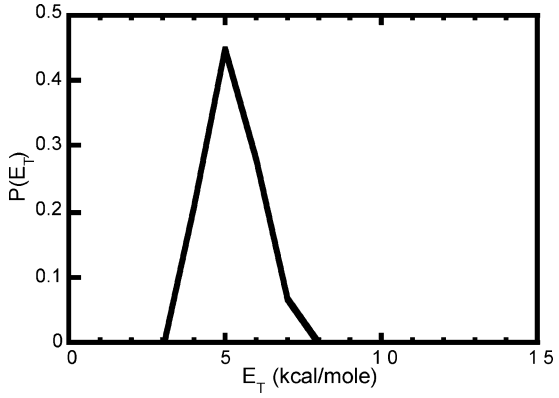

Figure 6. Recoil translational energy distribution of $CH_3O + CO$ in the dissociation of ground-state CH_3OCO radicals. The solid line shows the $P(E_T)$ used for the dissociation dynamics of the radicals, produced in the C−Cl fission of the precursor that produces ground-state radicals via the $P(E_T)$ in the solid black line of Figure 4, to fit the CO^+ and HCO^+ data in Figures 5 and 8, respectively.

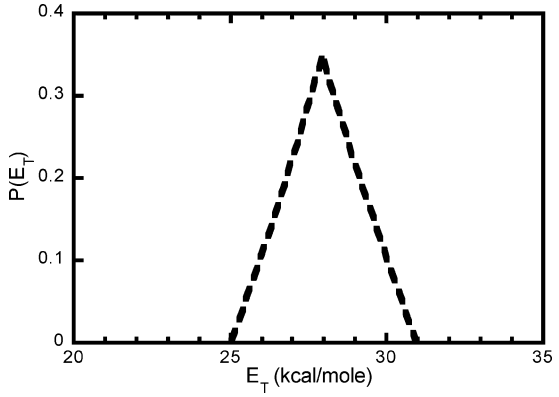

Figure 7. Recoil translational energy distribution of $CH_3O + CO$ in the dissociation of excited-state CH_3OCO radicals. The dashed line shows the $P(E_T)$, which gave a good fit to the CO^+ and HCO^+ data in Figures 5 and 8, respectively. The fitting also uses the velocity of the excited-state CH_3OCO as produced by the $P(E_T)$ in the dashed line of Figure 4.

the methoxy radical in reaction 2. It was impossible to gain a satisfactory fit of the data by assigning one $P(E_T)$ for the dissociation of the total distribution of CH_3OCO radicals shown by the gray line in Figure 4. This led us to believe that the low E_T CH_3OCO radicals, ∼15% of all the radical product, which are formed with high internal energy, are dissociating from an excited state and thus can exhibit different dissociation dynamics than the ground-state radicals. The thin solid line in Figure 5 shows CO produced from ground-state radical dissociation. These CO fragments recoil from methoxy radicals with a kinetic energy distribution shown by the solid line in Figure 6, and they originate from CH_3OCO radicals corresponding to the black solid line in Figure 4. Likewise, the dashed line in Figure 5 shows CO from dissociation of excited-state CH_3OCO radicals fit by the dashed lines of Figures 4 and 7. The dissociation of the excited-state CH_3OCO radicals to $CH_3O + CO$ likely occurs via electronic predissociation by a repulsive excited-state potential surface, as much higher energies are partitioned to recoil kinetic energy than in ground-state dissociation.

Figure 8 shows a $m/e = 29$ (HCO^+) TOF spectrum. The majority of the signal is due to dissociative ionization of CH_3O fragments produced as partners to CO in reaction 2. The CH_3O^+ ion is known to predissociate to $CHO^+ + H_2$ even at the zero point level, so $m/e = 29$ is the value at which we detect CH_3O products.[36] The data are momentum-matched to the CO^+ data

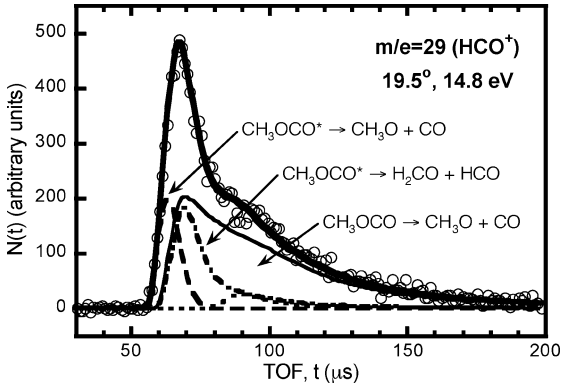

Figure 8. TOF spectrum of $m/e = 29$ (HCO^+) taken at a 19.5° source angle and 14.8 eV ionization energy for 100000 laser shots. Open circles are experimental data points, and the bold solid line is the overall fit to the data. CH_3O products, which dissociatively ionize to HCO^+, appear in this spectrum and are momentum-matched to CO fragments. The data are fit in an identical manner to the CO^+ data in Figure 5, with the solid and dashed lines showing products of reaction 2 for ground-state and excited-state CH_3OCO radicals, respectively. The dot−dashed line shows signal from HCO and dissociative ionization of H_2CO, assigned to reaction 4 for CH_3OCO radicals with high internal energy. This contribution is determined by the data in Figure 9, fit by the $P(E_T)$ in Figure 10. The dotted line shows a possible contribution from dissociative ionization of excited-state CH_3OCO radicals that may not dissociate before reaching the ionizer.

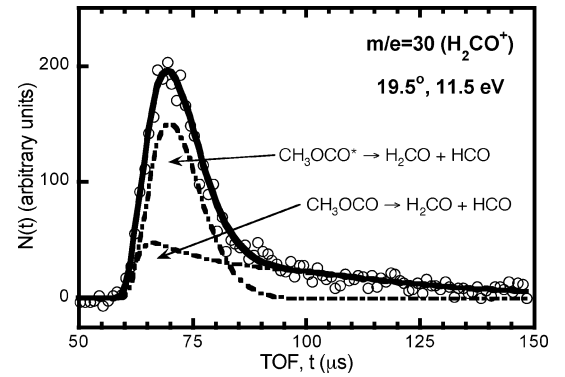

Figure 9. TOF spectrum of $m/e = 30$ (H_2CO^+) obtained from 200000 laser shots at a 19.5° source angle and 11.5 eV ionization energy. Open circles are experimental data and the solid line is the overall fit. The dot−dashed line in the TOF range of 60−90 μs is well-fit by excited-state CH_3OCO radicals dissociating with the $P(E_T)$ shown in Figure 10. The slower signal, shown by the dot−dashed line extending to 150 μs, could be due to high internal energy ground-state radicals dissociating with less than 10 kcal/mol partitioned into product recoil. Both of these contributions also appear in Figure 8.

in Figure 5 and are fit in an identical manner, with the thin solid line in Figure 8 showing CH_3O from dissociation of ground-state CH_3OCO and the dashed line showing CH_3O originating from excited-state radicals, fit by the corresponding $P(E_T)$s in Figures 4, 6 and 7. The dot−dashed line in Figure 8 shows HCO^+ signal from HCO and from dissociative ionization of H_2CO. The source of neutral HCO and H_2CO is explained directly below.

The presence of H_2CO was confirmed in a $m/e = 30$ (H_2CO^+) TOF spectrum (Figure 9); and is assigned to the minor dissociation of CH_3OCO radicals to $H_2CO + HCO$ (reaction 4). Note that the HCO and H_2CO products of reaction 4 would have essentially the same velocities as they differ by only one mass unit. The data are mostly fit by assignment to dissociation of excited-state radicals, as shown by the dot−dashed peak with an arrival time of 60−90 μs in Figure 9. An average of 15 kcal/mol is imparted in this step, as shown by the $P(E_T)$ in Figure

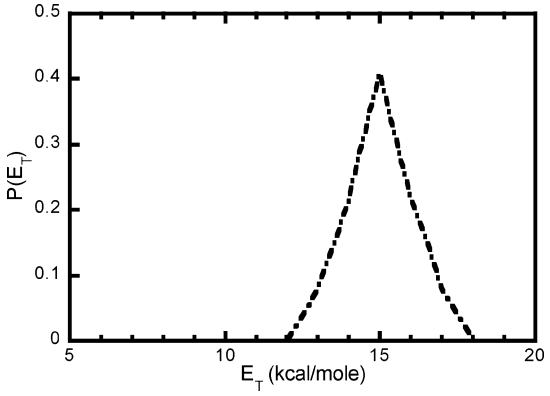

Figure 10. Recoil translational energy distribution for $CH_3OCO^* \rightarrow H_2CO + HCO$. The dot−dashed line shows the $P(E_T)$ determined from forward convolution fitting of the data in Figure 9, also used to fit the corresponding contribution in Figure 8.

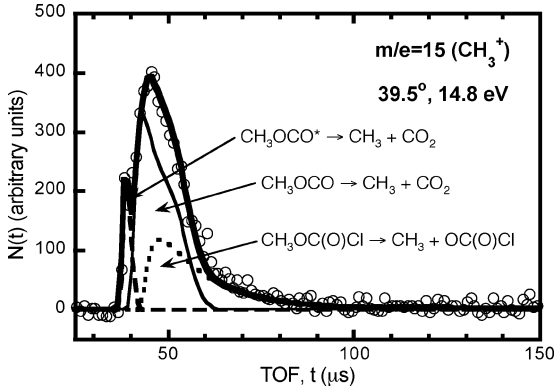

Figure 11. Preliminary fit of a $m/e = 15$ (CH_3^+) TOF spectrum taken at a 39.5° source angle and 14.8 eV ionization energy for 50000 laser shots. Open circles are experimental data points, and the bold solid line is the total fit to the data. The thin solid line shows CH_3 produced by unimolecular dissociation of ground-state CH_3OCO radicals with $E_{int} \geq 32$ kcal/mol, the predicted barrier to dissociation from ref 16. This signal is fit by the $P(E_T)$ distribution shown by the solid line in Figure 12. The dashed line shows CH_3 from excited-state CH_3OCO radicals, fit by the dashed lines in Figures 4 and 13. The dotted line is assigned to CH_3 produced by reaction 6 and fit by the $P(E_T)$ in Figure 14.

10. The tail in the $m/e = 30$ TOF spectrum could be accounted for by dissociation of ground-state radicals, using those radicals with E_{int} above Wang's G2//B3LYP barrier of 40 kcal/mol,[16] coming from C−Cl bond fission events imparting less than 25 kcal/mol in recoil kinetic energy. This contribution is shown by the lower dot−dashed line with arrival time extending to 150 μs in Figure 9, but is highly uncertain due to the overlap of the two contributions. It is difficult to be accurate in determining the $P(E_T)$ describing the dissociation of these ground-state radicals; an average recoil energy between 3 and 9 kcal/mol could provide a satisfactory fit. Reactions 8 and 11 can also produce H_2CO, but the signal for its cofragment at $m/e = 64$ is comparatively low. For a $m/e = 64$ ($HCOCl^+$) TOF spectrum taken at a source angle of 19.5° and an ionization energy of 14.8 eV for 75000 laser shots, the integrated signal was 597 ± 53 counts. Granted, it would be expected that a significant portion of the nascent HCOCl or HOCCl fragments would have sufficient internal energy to dissociate by reactions 9 or 12,[21] but we observed virtually no HCl^+ signal and no obvious contribution to the CO^+ TOF spectrum. Therefore, we conclude that reactions 8 and 11 are negligible channels in the precursor photodissociation.

Unimolecular dissociation of CH_3OCO radicals also produced significant amounts of CH_3 and CO_2 via reaction 3. Figure 11 shows the $m/e = 15$ (CH_3^+) TOF spectrum taken at a 39.5° source angle and an ionization energy of 14.8 eV. The thin solid line shows CH_3 produced by the dissociation of ground-state radicals. We first fit these data using the distribution of CH_3OCO radicals with internal energy above the G2(B3LYP/MP2/CC) predicted dissociation barrier of 32.3 kcal/mol calculated by Wang et al.[16] (Later in this paper we refit the data as we identified a second, lower transition state.) The fit accounts for the velocity imparted to the CH_3OCO radical in the initial C−Cl bond fission (reaction 1) as well as the velocity imparted during the recoil of CH_3 from CO_2 in reaction 3. Figure 12 shows the distribution of recoil kinetic energies imparted to the CH_3 and CO_2 fragments. Excited-state CH_3OCO radicals can also dissociate via reaction 3, as shown by the dashed line in Figure 11. The dissociation of these radicals is described by the $P(E_T)$ in Figure 13, which is used in conjunction with the dashed line of Figure 4 to predict the TOF distribution in Figure 11. A comparison of the CH_3 TOF distribution to that of CO_2 (Figure 15) revealed that the two signals are not completely momentum-matched, as would be expected if reaction 3 were the only source of CH_3 and CO_2. We concluded that there must be another source of CH_3^+ signal. The dotted line in Figure 11 shows signal from the initial photolysis of methyl chloroformate, reaction 6:

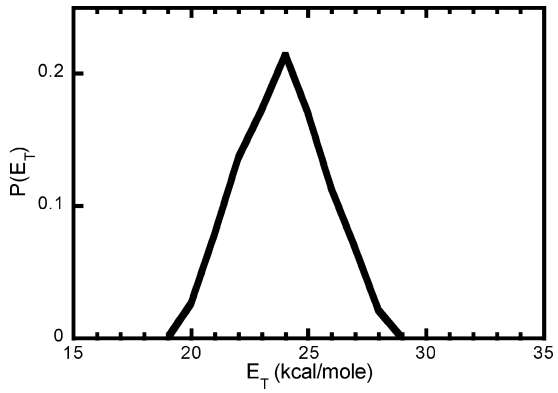

Figure 12. $P(E_T)$ describing the distribution of translational energies imparted during the recoil of CH_3 and CO_2 in the dissociation of ground-state CH_3OCO radicals.

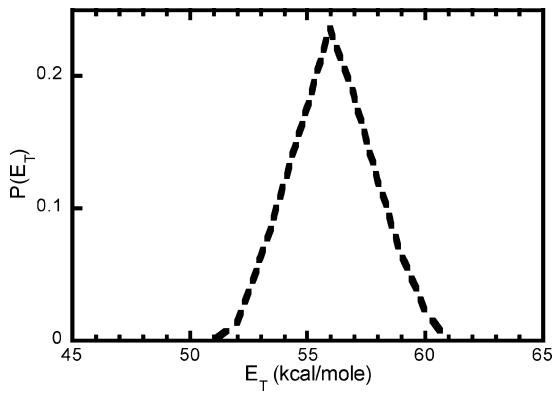

Figure 13. $P(E_T)$ describing the distribution of translational energies imparted during the recoil of CH_3 and CO_2 in the dissociation of excited-state CH_3OCO radicals.

$CH_3OC(O)Cl \rightarrow CH_3 + OC(O)Cl$. The $P(E_T)$ for this minor photolysis pathway is shown in Figure 14.

Figure 15 shows the $m/e = 44$ (CO_2^+) TOF spectrum obtained at a 19.5° source angle and 14.8 eV ionization energy. The thin solid and dashed lines show CO_2 produced in the unimolecular dissociation of ground- and excited-state CH_3OCO radicals, respectively. These distributions are momentum-matched to

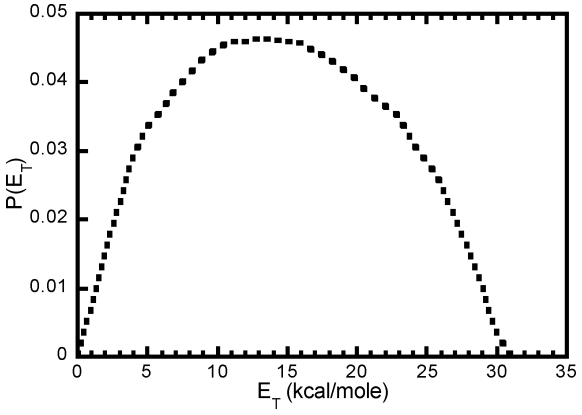

Figure 14. Recoil kinetic energy distribution in the initial photolytic step $CH_3OCOCl \rightarrow CH_3 + OCOCl$. This distribution produced the dotted line fit in Figure 11.

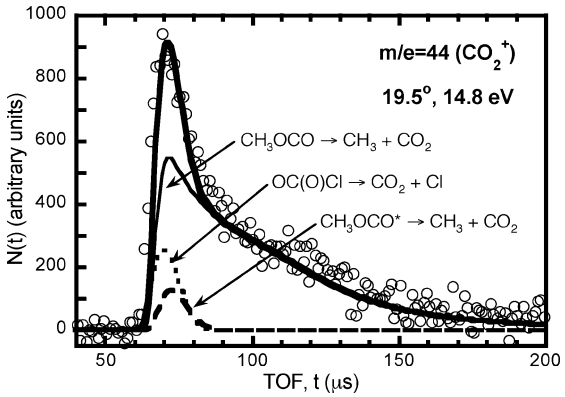

Figure 15. Preliminary fit of an experimental $m/e = 44$ (CO_2^+) TOF spectrum taken at a 19.5° source angle and 14.8 eV ionization energy for 150000 laser shots. Open circles are experimental data points and the bold solid line is the total fit to the data. The thin solid and dashed lines describe unimolecular dissociation of CH_3OCO radicals and are momentum-matched to those in the $m/e = 15$ TOF spectrum in Figure 11. The dotted line is assigned to CO_2 produced by dissociation of OCOCl radicals and fit by the $P(E_T)$ in Figure 16 in conjunction with the velocities of the OCOCl radical products from C−C bond fission in the precursor.

those of the CH_3^+ TOF in Figure 11 and are fit in an identical manner, using the $P(E_T)$s in Figures 4, 12 and 13. In the fitting of the CH_3^+ TOF, we also include a contribution from the $CH_3OC(O)Cl \rightarrow CH_3 + OC(O)Cl$ photolysis channel. The OC(O)Cl radical has a predicted dissociation barrier of 2 kcal/mol.[20] Thus, we can reasonably expect the full distribution of OC(O)Cl to be unstable and produce CO_2 + Cl. We show this contribution to the CO_2^+ TOF by the dotted line and fit it using the $P(E_T)$ in Figure 16 in conjunction with that of Figure 14.

The magnitude of the observed CH_3 and CO_2 signal is surprising, given the high barrier of reaction 3 relative to reaction 2 predicted in the previous ab initio methods summarized in Figure 1. To investigate this phenomenon, we executed RRKM calculations[37] to predict rate constants for the two dissociation channels of CH_3OCO for energies between 21 and 59 kcal/mol, which correspond to the internal energy range of ground-state radicals produced in our experiments. The calculations used vibrational frequencies and rotational constants for the radical and transition states taken from the G2//B3LYP results of Wang et al.[16] Figure 17 reports energy-specific branching fractions derived from the RRKM calculations when the external moments of inertia are treated as adiabatic and the torsional mode associated with rotation of the methyl group is treated as a free

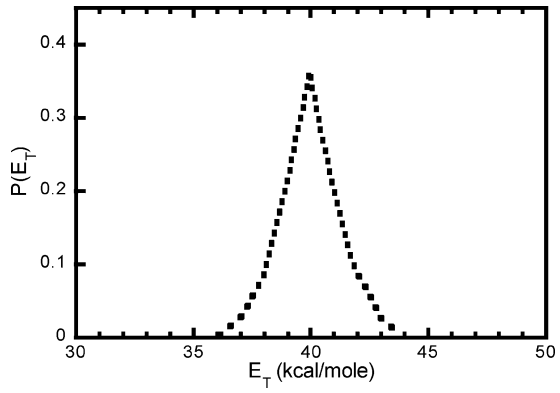

Figure 16. $P(E_T)$ describing the distribution of translational energies imparted during the recoil of CO_2 and Cl in the dissociation of OCOCl radicals.

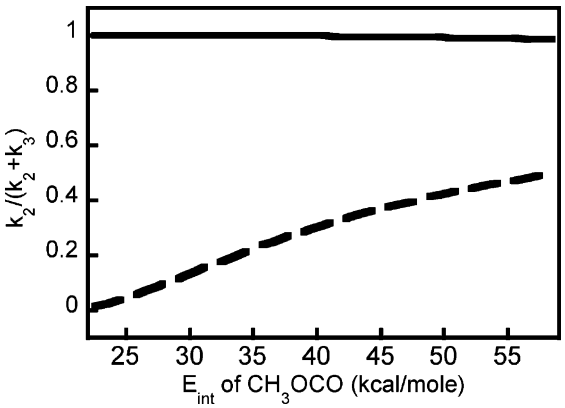

Figure 17. RRKM predictions for the unimolecular dissociation of ground-state CH_3OCO radicals. The label k_2 refers to the rate constant for reaction 2 (CH_3O + CO products) and k_3 refers to reaction 3 (CH_3 + CO_2 products). The solid line shows $k_2/(k_2 + k_3)$ calculated using the frequencies, moments of inertia and transition state energies predicted by Wang et al. in ref 16. The dashed line shows $k_2/(k_2 + k_3)$ calculated using the parameters for the new, lower-energy transition state predicted in this work. The rate constants were calculated for the internal energy range of the ground-state radicals produced in our experiments.

internal rotor. The solid line in Figure 17 shows that branching to the CH_3O + CO products is heavily favored, based on RRKM calculations using the transition states of Wang et al. The dashed line in Figure 17 will be discussed below. The RRKM results are presented with the caveat that some of the higher internal energy radicals are in a low-lying excited state of CH_3OCO; the RRKM calculations are not relevant to the dissociation of the excited-state radicals.

The RRKM calculations, using the transition states of Wang et al., predicted a CO/CO_2 branching ratio of 280:1 for the dissociation of ground-state radicals in our experiment. Because the E_{int} distribution of the radicals is broad, the branching ratio was calculated in the following way. For each internal energy, an energy-specific branching fraction was found. Each energy-specific branching fraction was multiplied by the fraction of radicals with that E_{int} calculated by integrating the measured $P(E_T)$ in Figure 4 over the corresponding E_T range at increments of 1 kcal/mol. The results were summed over the energies for ground-state radicals and then the ratio for CO/CO_2 was calculated.

An experimental branching ratio of 1:2.5 was determined by comparison of the signal attributed to dissociation of ground-state radicals in the CO and CO_2 TOF spectra. The spectra were taken under identical beam conditions, with the same source

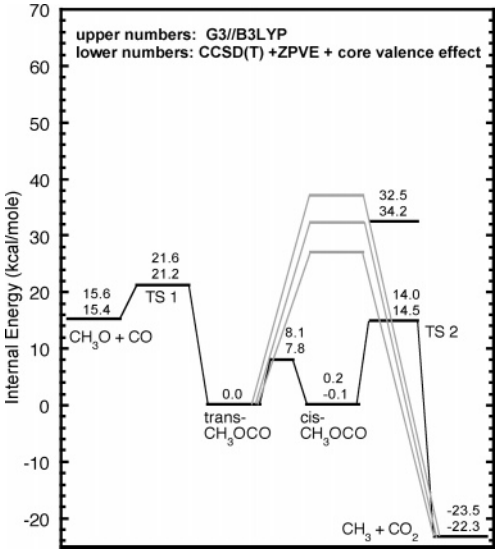

Figure 18. Energetics of the $CH_3O + CO \rightarrow CH_3 + CO_2$ reaction calculated by G3//B3LYP and CCSD(T) methods in this work. Included is the isomerization barrier for the CH_3OCO radical and the energies for both the cis and trans conformers of the transition state for the $CH_3 + CO_2$ product channel. The gray lines show the previously calculated energies for the trans conformer of the same transition state, which were also shown and referenced in Figure 1.

angle, ionization energy and number of laser shots. The experimental branching ratio R was found as follows:

$$R = \frac{\sigma_{CH_3O + CO}}{\sigma_{CH_3 + CO_2}} = \frac{CO^+ \text{ signal}}{CO_2{}^+ \text{ signal}} \frac{\text{expected signal } (CO_2)}{\text{expected signal (CO)}} \frac{\sigma_{ion}(CO_2)}{\sigma_{ion}(CO)} \frac{f_{CO_2{}^+/CO_2}}{f_{CO^+/CO}}$$

$$R = \frac{\sigma_{CH_3O + CO}}{\sigma_{CH_3 + CO_2}} = \frac{6441 \text{ counts}}{4576 \text{ counts}} \frac{11258 \text{ counts}}{21098 \text{ counts}} \frac{12 \text{ Mb}}{22.7 \text{ Mb}} \frac{1}{1} = \frac{1}{2.5}$$

Here we integrate the spectra in the range 61.4−89.4 μs for the CO^+ data and 77.4−96.4 μs for the $CO_2{}^+$ data. The expected signals are the predicted integrated signals in the same TOF ranges when it is assumed that the CO/CO_2 branching is 1:1, thus, they correct for the kinematic factors and Jacobians in the fitting of the data. The photoionization cross sections of the two products, σ_{ion}, are estimated by using the literature cross sections of room-temperature CO and CO_2 molecules[38,39] while f represents the percentage of the ionized product that is detected at its parent mass. In this case, $f = 1$ for both products because the photoionization energy used was below the appearance energies for daughter ions of both CO and CO_2.[40]

The large discrepancy in the theoretical (280:1) and experimental (1:2.5) product branching ratios led us to reevaluate the transition state for the $CH_3 + CO_2$ product channel. Our G3//B3LYP and CCSD(T) calculations revealed an additional transition state that is 18 kcal/mol lower than that predicted by Wang et al. The main difference lies in the geometry of the transition state. Wang et al. showed a transition state with trans geometry relative to the O−C bond. In fact, all of the published papers discussed thus far identified only the trans conformer of the transition state.[13−18] Our predicted transition state with lower energy has a cis geometry. Figure 18 shows our calculated transition state energy, along with energetics and isomerization

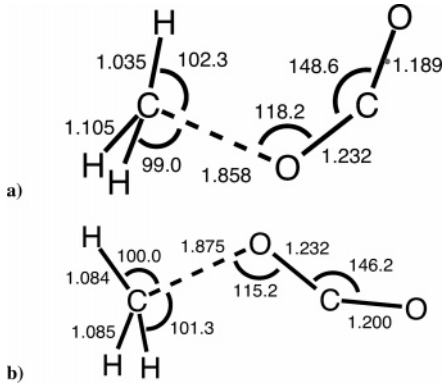

Figure 19. G3//B3LYP geometries for the (a) cis and (b) trans conformations of the transition state for the $CH_3OCO \rightarrow CH_3 + CO_2$ reaction. Bond lengths are in angstroms and angles are in degrees.

TABLE 2: Vibrational Frequencies and Moments of Inertia for Transition States Calculated at the B3LYP/6-311G(2df,p) Level of Theory

	moments of inertia (amu·Å^2)	frequencies (cm^{-1})
trans-CH_3OCO	8.492, 107.443, 112.718	17, 219, 319, 621, 995, 1122, 1174, 1221, 1477, 1493, 1500, 1882, 3051, 3126, 3156
TS1 (CH_3O + CO channel)	11.822, 138.223, 146.729	300i, 94, 154, 201, 323, 1000, 1125, 1151, 1413, 1415, 1515, 2151, 2959, 3016, 3048
TS2 (CH_3 + CO_2 channel)	22.703, 94.575, 113.890	740i, 49, 190, 507, 671, 778, 788, 1064, 1180, 1436, 1440, 2034, 3106, 3258, 3265

TABLE 3: Product Branching Ratios, *R*, Obtained from RRKM Predictions and Experimental Data

method	$R = \sigma_{CH_3O + CO}/\sigma_{CH_3 + CO_2}$
RRKM using transition states from ref 16	280/1
RRKM using transition states from this work	1/2
Experimental	$1/(2.5 \pm 0.5)$

barriers for the $CH_3O + CO$ reaction, on the same scale as previous theoretical predictions. Figure 19 shows the G3//B3LYP geometries of both the cis and trans transition state conformers. The critical implication of our results is that the lowest-energy barrier to dissociation of the CH_3OCO radical actually leads to $CH_3 + CO_2$, not $CH_3O + CO$. We executed RRKM calculations using the vibrational frequencies and moments of inertia in Table 2. The dashed line in Figure 17 shows that the $CH_3O + CO$ channel is not dominant; rather, the $CH_3 + CO_2$ channel is favored for the range of $E_{int} = 21$ to 59 kcal/mol with our calculated transition states. We ignored the contribution of $CH_3OCO \rightarrow CH_3 + CO_2$, which proceeds through the trans conformation of the transition state found by Wang et al., as it would make a negligible addition to the total $CH_3 + CO_2$ product branching. Table 3 summarizes the branching ratios determined by RRKM calculations using the two different transition states, as well as our experimentally measured branching ratio.

Assuming our transition states are indeed correct, it is necessary to revise the fitting of our CH_3 and CO_2 TOF data. With the lower barrier to the $CH_3 + CO_2$ channel, the entire internal energy range of the nascent CH_3OCO radicals lies above the energy barriers to both reactions 2 and 3. Therefore, we ought to fit the CH_3 and CO_2 data using the full distribution of

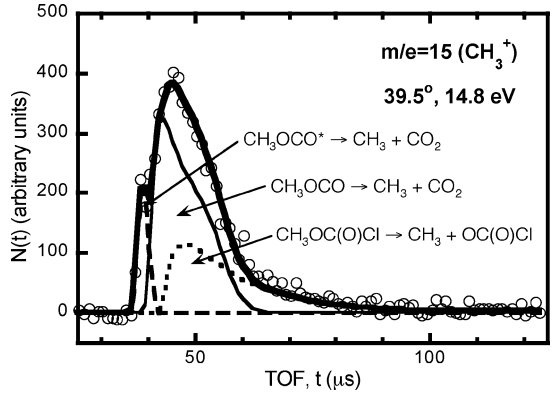

Figure 20. Refit $m/e = 15$ (CH_3^+) TOF spectrum. The data and fit are identical to that of Figure 11, except that the full distribution of ground-state radicals from Figure 4 is considered, as we now know that the energy barrier to reaction 3 is lower than previously thought.

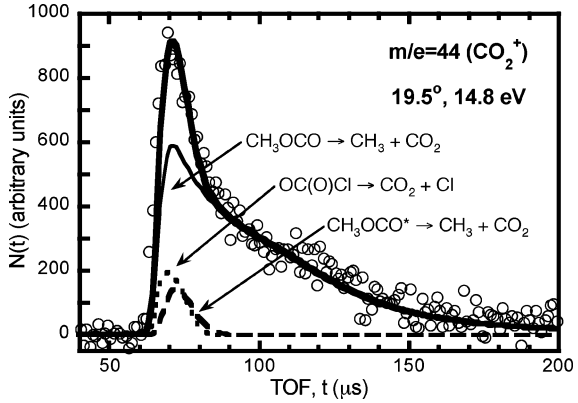

Figure 21. Refit $m/e = 44$ (CO_2^+) TOF spectrum. The data and fit are identical to that of Figure 15, except that the full distribution of ground-state radicals from Figure 4 is considered, as we now know that the energy barrier to reaction 3 is lower than previously thought.

radicals represented in Figure 4, appropriately weighted across the distribution so that it accounts for the fact that the $CH_3 + CO_2$ products dominate from the high E_T, low E_{int}, portions of the $P(E_T)$ in Figure 4. Figures 20 and 21 show the refit CH_3^+ and CO_2^+ TOF spectra, respectively.

Discussion

Photolysis of methyl chloroformate at 193 nm resulted in C−Cl bond fission, along with C−C bond fission and a minor H_2CO elimination channel. C−Cl bond fission produced CH_3OCO radicals with sufficient energy to overcome dissociation barriers to both the $CH_3O + CO$ and the $CH_3 + CO_2$ product channels. The branching to the $CH_3 + CO_2$ channel is much larger than the predicted branching based on previous transition state calculations. Our own calculations found another transition state for the $CH_3 + CO_2$ channel, which is consistent with our experimentally observed branching ratio. This transition state has a cis conformation with significantly lower energy than the trans conformer. The situation is very similar to that of the HOCO radical, which has two transition states leading to $H + CO_2$ products. The *cis*-HOCO transition state is predicted to be 6.4 kcal/mol lower than the *trans*-HOCO transition state.[3] The same ordering of cis and trans dissociation barriers is seen in the $CO + SO_2 \rightarrow CO_2 + SO$ reaction.[41] A more general description of this trend is that the breaking bond of the radical is trans relative to the radical electron. This is the case when the vinyl radical dissociates to H + acetylene[42] and also when the 2-buten-2-yl radical accesses its C−C and C−H bond fission channels.[43]

The overall photolysis of methyl chloroformate is complex, with overlapping signal from several different channels making data analysis difficult. Performing these experiments with a longer photolysis wavelength would be advantageous in that the nascent CH_3OCO radicals would have lower internal energy, possibly avoiding formation of excited-state radicals. Such an experiment would also enable an experimental determination of the lowest barrier to dissociation of the CH_3OCO radical, which we predict as belonging to reaction 3. We did attempt these experiments using 248 nm photolysis of methyl chloroformate, but the absorption (Figure 2) is too low to yield sufficient signal. Preliminary velocity-map imaging experiments in our group showed that 235 nm photolysis produces CH_3OCO radicals with an internal energy range that spans both barriers to dissociation. If this photolysis wavelength is coupled with detection of stable CH_3OCO radicals, it would be possible to determine the lowest barrier to dissociation. This could be done by measuring the translational energy distribution for the stable radicals and comparing it to the full C−Cl bond fission $P(E_T)$.

Both the $CH_3 + CO_2$ and $CH_3O + CO$ channels are peculiar in that they could not be fit simply by the $P(E_T)$ for initial C−Cl bond fission coupled with a single secondary $P(E_T)$ for the kinetic recoil of the final product fragments. The data required two drastically different $P(E_T)$s to describe the recoil products from the high- and low- internal energy CH_3OCO radicals, respectively. This suggests that there are two different mechanisms at work, leading us to assign low E_T, high E_{int} CH_3OCO radicals to an excited state. The experiments show that the excited state has an adiabatic excitation energy of at most 55 kcal/mol. There are currently no published theoretical studies that treat the low-lying excited states of the radical.

The experimental results presented here and the theoretical predictions summarized in Figure 18 offer insight into the $CH_3O + CO$ bimolecular addition reaction. Although a handful of kinetics studies have been published for the $CH_3O + CO$ reaction, the recommended study[10] derives an Arrhenius expression from data over a narrow temperature range, so one cannot be assured the expression is in the high-pressure limit. There is, however, good agreement among various theoretical methods regarding the entrance channel barrier, but no experimental test. Now that our own calculations have revealed new features of the potential energy surface, it may be worthwhile to revisit $CH_3O + CO$ kinetics experiments. One caution in applying the results of this paper to the $CH_3O + CO$ bimolecular reaction is that our experiments can only reveal the portion of the dynamics that would proceed via the radical intermediate. Though the CH_3OCO intermediate has been consistently predicted by theory, a direct pathway to $H_2CO + HCO$ has also been identified.[15,16] The technique used in this paper cannot probe such direct reactions, nor would it easily lend itself to determination of the $CH_3OCO \rightarrow CH_3O + CO$ energy barrier as our results have shown that it is not the lowest barrier to dissociation of the radical. It could, however, prove useful for experimental verification of the $CH_3OCO \rightarrow CH_3 + CO_2$ barrier.

After we submitted this paper and presented the work at national conferences, another recent paper concerning CH_3OCO was brought to our attention. Glaude et al.[44] have studied the chemical kinetics of dimethyl carbonate (DMC), a compound of interest as an oxygenate additive for diesel fuel. The CH_3OCO radical is a key intermediate in the decomposition of DMC, so the ultimate fate of CH_3OCO radicals is important to the effectiveness of DMC as an oxygenate. Measurements of product mole fractions in an opposed-flow diffusion flame of

DMC showed a majority of CO_2 and a minor amount of CO. The paper includes an estimate of the product branching using transition states for both reactions calculated with the CBS-Q method; they predicted the product branching for CH_3OCO decomposition to be 78% to $CH_3 + CO_2$ (14.7 kcal/mol barrier), and 22% to $CH_3O + CO$ (22.7 kcal/mol barrier) at 1100 K. The Glaude paper also references previous work by Good and Francisco[45] that includes a recalculation of the transition state for $CH_3OCO \rightarrow CH_3 + CO_2$ with a barrier height of 14.7 kcal/mol and a *cis*- conformation in agreement with our results. This paper by Good and Francisco was not found in our initial literature searches nor referenced in other recent ab initio studies[14,15,17] cited in the present work.

Acknowledgment. This work was supported by the Chemical, Geosciences and Biosciences Division, Office of Basic Energy Sciences, Office of Science, U.S. Department of Energy, under Grant No. DE-FG02-92ER14305 (L.J.B.). Synchrotron beamtime and additional funding were provided by the National Synchrotron Radiation Research Center and Academia Sinica in Taiwan (J.J.L.). L.R.M. was partially supported by a U.S. Department of Education GAANN Fellowship and a Sigma Xi Grant in Aid of Research. The MOLPRO calculations in this work were performed using the Molecular Science Computing Facility (MSCF) in the William R. Wiley Environmental Molecular Sciences Laboratory, a national scientific user facility sponsored by the U. S. Department of Energy's Office of Biological and Environmental Research. The Gaussian 03 calculations in this work used resources of the National Energy Research Scientific Computing Center, which is supported by the Office of Science of the U.S. Department of Energy under Contract No. DE-AC03-76SF00098. The authors thank Shih-Huang Lee and Chanchal Chaudhuri for technical assistance during the experiments. Doran Bennett is acknowledged for executing the Gaussian 98 G3//B3LYP calculations reported here for reactions 6, 8, and 11. Marie Justine Bell is acknowledged for assistance in collecting the absorption spectrum of methyl chloroformate. The students and faculty on this paper wish to thank Bill Hase for the wonderful scientific insights in his text on chemical kinetics and dynamics; we hope he enjoys that this paper used his original RRKM code!

References and Notes

(1) Steinfeld, J. I.; Francisco, J. S.; Hase, W. L. *Chemical Kinetics and Dynamics*; Prentice Hall, Inc.: Upper Saddle River, NJ, 1989.

(2) Seinfeld, J. H.; Pandis, S. N. *Atmospheric Chemistry and Physics: From Air Pollution to Climate Change*; John Wiley & Sons: New York, 1998.

(3) Yu, H.-G.; Muckerman, J. T.; Sears, T. J. *Chem. Phys. Lett.* **2001**, *349*, 547.

(4) Kudla, K.; Schatz, G. C.; Wagner, A. F. *J. Chem. Phys.* **1991**, *95*, 1635.

(5) Golden, D. M.; Smith, G. P.; McEwen, A. B.; Yu, C.-L.; Eiteneer, B.; Frenklach, M.; Vaghjiani, G. L.; Ravishankara, A. R.; Tully, F. P. *J. Phys. Chem. A* **1998**, *102*, 8598.

(6) Lester, M. I.; Pond, B. V.; Marshall, M. D.; Anderson, D. T.; Harding, L. B.; Wagner, A. F. *Faraday Discuss.* **2001**, *118*, 373.

(7) Clements, T. G.; Continetti, R. E.; Francisco, J. S. *J. Chem. Phys.* **2002**, *117*, 6478.

(8) Wiebe, H. A.; Heicklen, J. *J. Am. Chem. Soc.* **1973**, *95*, 1.

(9) Sanders, N.; Butler, J. E.; Pasternack, L. R.; McDonald, J. R. *Chem. Phys.* **1980**, *48*, 203.

(10) Lissi, E. A.; Massiff, G. *J. Chem. Soc., Faraday Trans. 1* **1973**, *69*, 346.

(11) Wantuck, P. J.; Oldenborg, R. C.; Baughcum, S. L.; Winn, K. R. *Chem. Phys. Lett.* **1987**, *138*, 548.

(12) Tsang, W.; Hampson, R. F. *J. Phys. Chem. Ref. Data* **1986**, *15*, 1087.

(13) Francisco, J. S. *Chem. Phys.* **1998**, *237*, 1.

(14) Kang, J. K.; Musgrave, C. B. *J. Chem. Phys.* **2001**, *115*, 11040.

(15) Zhou, Z.; Cheng, X.; Zhou, X.; Fu, H. *Chem. Phys. Lett.* **2002**, *353*, 281.

(16) Wang, B.; Hou, H.; Gu, Y. *J. Phys. Chem. A* **1999**, *103*, 8021.

(17) Hou, H.; Wang, B.; Gu, Y. *Phys. Chem. Chem. Phys.* **2000**, *2*, 2329.

(18) Mebel, A. M.; Diau, E. W. G.; Lin, M. C.; Morokuma, K. *J. Am. Chem. Soc.* **1996**, *118*, 9759.

(19) Frisch, M. J.; Trucks, G. W.; Schlegel, H. B.; Scuseria, G. E.; Robb, M. A.; Cheeseman, J. R.; Zakrzewski, V. G.; Montgomery, J. A., Jr.; Stratmann, R. E.; Burant, J. C.; Dapprich, S.; Millam, J. M.; Daniels, A. D.; Kudin, K. N.; Strain, M. C.; Farkas, O.; Tomasi, J.; Barone, V.; Cossi, M.; Cammi, R.; Mennucci, B.; Pomelli, C.; Adamo, C.; Clifford, S.; Ochterski, J.; Petersson, G. A.; Ayala, P. Y.; Cui, Q.; Morokuma, K.; Malick, D. K.; Rabuck, A. D.; Raghavachari, K.; Foresman, J. B.; Cioslowski, J.; Ortiz, J. V.; Stefanov, B. B.; Liu, G.; Liashenko, A.; Piskorz, P.; Komaromi, I.; Gomperts, R.; Martin, R. L.; Fox, D. J.; Keith, T.; Al-Laham, M. A.; Peng, C. Y.; Nanayakkara, A.; Gonzalez, C.; Challacombe, M.; Gill, P. M. W.; Johnson, B. G.; Chen, W.; Wong, M. W.; Andres, J. L.; Head-Gordon, M.; Replogle, E. S.; Pople, J. A. *Gaussian 98*, revision A.11.3; Gaussian, Inc.: Pittsburgh, PA, 1998.

(20) Francisco, J. S.; Goldstein, A. N. *Chem. Phys.* **1988**, *127*, 73.

(21) Francisco, J. S.; Zhao, Y. *J. Chem. Phys.* **1992**, *96*, 7587.

(22) Chase, M. W. *J. Phys. Chem. Ref. Data Monogr.* **1998**, *9*, 1−1951.

(23) Francisco, J. S.; Williams, I. H. *J. Am. Chem. Soc.* **1993**, *115*, 3746.

(24) Lin, J. J.; Chen, Y.; Lee, Y. Y.; Lee, Y. T.; Yang, X. *Chem. Phys. Lett.* **2002**, *361*, 374.

(25) Baboul, A. G.; Curtiss, L. A.; Redfern, P. C.; Raghavachari, K. *J. Chem. Phys.* **1999**, *110*, 7650.

(26) Hampel, C.; Peterson, K. A.; Werner, H. *Chem. Phys. Lett.* **1990**, *190*, 1.

(27) Deegan, M. J. O.; Knowles, P. J. *Chem. Phys. Lett.* **1994**, *227*, 321.

(28) Knowles, P. J.; Hampel, C.; Werner, H. J. *J. Chem. Phys.* **1988**, *99*, 5219.

(29) Dunning, T. H., Jr. *J. Chem. Phys.* **1989**, *90*, 1007.

(30) Dunning, T. H., Jr.; Peterson, K. A.; Wilson, A. K. *J. Chem. Phys.* **2001**, *114*, 9244.

(31) Peterson, K. A.; Dunning, T. H., Jr. *J. Chem. Phys.* **2002**, *117*, 10548.

(32) Frisch, M. J.; Trucks, G. W.; Schlegel, H. B.; Scuseria, G. E.; Robb, M. A.; Cheeseman, J. R.; Montgomery, J. A., Jr.; Vreven, T.; Kudin, K. N.; Burant, J. C.; Millam, J. M.; Iyengar, S. S.; Tomasi, J.; Barone, V.; Mennucci, B.; Cossi, M.; Scalmani, G.; Rega, N.; Petersson, G. A.; Nakatsuji, H.; Hada, M.; Ehara, M.; Toyota, K.; Fukuda, R.; Hasegawa, J.; Ishida, M.; Nakajima, T.; Honda, Y.; Kitao, O.; Nakai, H.; Klene, M.; Li, X.; Knox, J. E.; Hratchian, H. P.; Cross, J. B.; Bakken, V.; Adamo, C.; Jaramillo, J.; Gomperts, R.; Stratmann, R. E.; Yazyev, O.; Austin, A. J.; Cammi, R.; Pomelli, C.; Ochterski, J. W.; Ayala, P. Y.; Morokuma, K.; Voth, G. A.; Salvador, P.; Dannenberg, J. J.; Zakrzewski, V. G.; Dapprich, S.; Daniels, A. D.; Strain, M. C.; Farkas, O.; Malick, D. K.; Rabuck, A. D.; Raghavachari, K.; Foresman, J. B.; Ortiz, J. V.; Cui, Q.; Baboul, A. G.; Clifford, S.; Cioslowski, J.; Stefanov, B. B.; Liu, G.; Liashenko, A.; Piskorz, P.; Komaromi, I.; Martin, R. L.; Fox, D. J.; Keith, T.; Al-Laham, M. A.; Peng, C. Y.; Nanayakkara, A.; Challacombe, M.; Gill, P. M. W.; Johnson, B.; Chen, W.; Wong, M. W.; Gonzalez, C.; Pople, J. A. *Gaussian 03*, revision B.05; Gaussian, Inc.: Wallingford, CT, 2004.

(33) MOLPRO is a package of ab initio programs written by Werner, H.-J.; Knowles, P. J.; Schütz, M.; Lindh, R.; Celani, P.; Korona, T.; Rauhut, G.; Manby, F. R.; Amos, R. D.; Bernhardsson, A.; Berning, A.; Cooper, D. L.; Deegan, M. J. O.; Dobbyn, A. J.; Eckert, F.; Hampel, C.; Hetzer, G.; Lloyd, A. W.; McNicholas, S. J.; Meyer, W.; Mura, M. E.; Nicklass, A.; Palmieri, P.; Pitzer, R.; Schumann, U.; Stoll, H.; Stone, A. J.; Tarroni, R.; Thorsteinsson, T.

(34) Hansen, J. C.; Francisco, J. S.; Szente, J. J.; Maricq, M. M. *Chem. Phys. Lett.* **2002**, *365*, 267.

(35) Davies, P. B.; Russell, D. K. *Chem. Phys. Lett.* **1979**, *67*, 440.

(36) Kuo, S.-C.; Zhang, Z.; Klemm, R. B.; Liebman, J. F.; Stief, L. J.; Nesbitt, F. L. *J. Phys. Chem.* **1994**, *98*, 4026.

(37) Hase, W. L.; Bunker, D. L. *QCPE* **1974**, *234*.

(38) Shaw, D. A.; Holland, D. M. P.; Hayes, M. A.; MacDonald, M. A.; Hopkirk, H.; McSweeney, S. M. *Chem. Phys.* **1995**, *198*, 381.

(39) Veseth, L. *Phys. Rev. A* **1994**, *49*, 939.

(40) Lias, S. G.; Levin, R. D.; Kafafi, S. A. Ion Energetics Data. In *NIST Chemistry WebBook, NIST Standard Reference Database Number 69*; Linstrom, P. J., Mallard, W. G., Eds.; National Institute of Standards and Technology: Gaithersburg, MD, 2005.

(41) Bacskay, G. B.; Mackie, J. C. *J. Phys. Chem. A* **2005**, *109*, 2019.

(42) Harding, L. B.; Wagner, A. F.; Bowman, J. M.; Schatz, G. C. *J. Phys. Chem.* **1982**, *86*, 4312.

(43) Miller, J. L. *J. Phys. Chem. A* **2004**, *108*, 2268.

(44) Glaude, P. A.; Pitz, W. J.; Thomson, M. J. *Proc. Combust. Inst.* **2005**, *30*, 1111.

(45) Good, D. A.; Francisco, J. S. *J. Phys. Chem. A* **2000**, *104*, 1171.